# 4 Simulation

In Chapter 2, we obtained the results that the quench propagation velocity and current redistribution also depend on the contact electrical conductance between strands. We found that the field gradient across the cable cross section influenced the current redistribution during quench propagation. In order to examine the influence of current redistribution on the quench propagation velocity in more detail, a numerical simulation was performed. To simplify the simulation, we consider a model with two-parallel strands connected electrically and thermally. This chapter presents the description of the model and simulation results.

## 4.1 Model

Figure 4.1 shows the two-parallel strand model. The parameters of strands for the simulation are the same as those used in the experiment discussed in Chapter 2, and shown in Table 2.1. Two strands are in contact electrically with each other, and the strands are shorted electrically at the end of the cable. Therefore, the current can flow between the strands and at the both ends. Although generated heat can also transfer between the strands, it is neglected in order to pay attention only to the current redistribution. For the same reason, the cooling effect by liquid helium is also neglected. Namely, the calculation is performed under an adiabatic condition. The total current $I_{total}$ is kept constant during a quench process. A quench is initiated at the center of strand 1. The total length of the cable is 3.1 m. Since the actual Rutherford cable is twisted, strands in the cable are exposed to a varying magnetic field with the period of a cable twist pitch. For the simulation, this fact is simulated by applying the periodic change of a magnetic field to the strands.

## 4.2 Method

The two basic equations for simulating the quench propagation are a thermal equilibrium equation and an electrical circuit equation. These equations are solved step by step numerically, and the temperature and current distributions are obtained at every time step. In an actual calculation, since the current distribution and quench propagation are symmetric with respect to the quench origin, the calculation is done only in a half length of the cable.

The calculation procedure is as follows [37]:

1. the temperature distribution is calculated with the thermal equilibrium equations,
2. the resistance distribution is determined from the temperature distribution,
3. the current distribution is calculated with the electrical circuit equation using the resistance obtained above,
4. the Joule heat generation is determined from the current and resistance,
5. the time is advanced by one time step, and
6. the calculation is repeated from the first procedure.

### 4.2.1 Thermal Equilibrium Equation

It is assumed that the thermal propagation in a strand is in one dimension. In this case, all the material properties are averaged over the strand cross section. Including the Joule heat generation owing to the current redistribution through the electrical conductance between strands in Eq. (1.3), the thermal equilibrium equation for a strand is given by

$$\frac{\partial}{\partial x}\left(\kappa\frac{\partial T}{\partial x}\right) + g + g_c = C_p\frac{\partial T}{\partial t}, \tag{4.1}$$

where $g_c$ is the Joule heat generation at the electrical contact conductance between strands. The cooling effect by liquid helium and the heat transfer between strands are neglected as described before. The partial differential equation is solved by the Crank-Nicholson method, and the temperature distribution of the strands is obtained at every

time step.

The Joule heat generation $g$ is given by

$$g = \rho J^2, \tag{4.2}$$

where $\rho$ is the average resistivity over the strand cross section and $J$ is the strand current density. $\rho$ equals 0 when the strand is completely superconducting. The details of the resistivity $\rho$ will be shown in Section 4.2.3.

The Joule heat generation at the electrical contact conductance $g_c$ is calculated from the transferred current between strands and electrical contact conductance. The equation is described in the next section.

### 4.2.2 Electrical Circuit Equation

The electrical circuit of two-parallel strands is shown in Fig. 4.2 [38]. In order to regard a distributed constant circuit as a lumped element circuit, the cable is divided into small elements, $-n_{max}, ...., -1; 0, 1, ...., n_{max}$. Because of the symmetry with respect to element 0, the actual calculation is performed from element 0 to element $n_{max}$. Each element consists of a resistance and an inductance, and elements are connected by contact resistors. The circuit equation representing the loop at element $i$ is given by

$$\begin{aligned} R_{(1,i)}I_{(1,i)} - R_{(2,i)}I_{(2,i)} + R_c I_{c(i)} - R_c I_{c(i-1)} \\ + \sum_{j,k=1,0}^{2,n} \left\{ (M_{(1,i)(j,k)} - M_{(2,i)(j,k)}) \frac{dI_{(j,k)}}{dt} \right\} = 0, \end{aligned} \tag{4.3}$$

$$I_{c(i)} = I_{(1,i)} - I_{(1,i+1)}, \text{ and} \tag{4.4}$$

$$I_{total} = I_{(1,i)} + I_{(2,i)}, \tag{4.5}$$

where $R_{(1,i)}$ and $R_{(2,i)}$ are the resistance of strands 1 and 2 at element $i$, $I_{(1,i)}$ and $I_{(2,i)}$ are the currents of strands 1 and 2 at element $i$, $R_c$ is the contact resistance, $I_{c(i)}$ is the current transfer through $R_c$ at element $i$, and $M_{(1,i)(j,k)}$ and $M_{(2,i)(j,k)}$ are the mutual inductance between element $i$ of strands 1 and 2 and element $k$ of strand $j$. When $(j,k) = (1,i)$ or $(2,i)$, i.e. $M_{(1,i)(1,i)}$ or $M_{(2,i)(2,i)}$, $M$ is the self inductance.

Since the calculation model is symmetrical with respect to element 0, Eq. (4.3) should be modified slightly. For element $i = 0$, since $I_{c(-1)} = -I_{c(0)}$, Eq. (4.3) is rewritten as

$$R_{(1,0)}I_{(1,0)} - R_{(2,0)}I_{(2,0)} + 2R_cI_{c(0)} + \sum_{j,k=1,0}^{2,n}\left\{(M_{(1,0)(j,k)} - M_{(2,0)(j,k)})\frac{dI_{(j,k)}}{dt}\right\} = 0. \quad (4.6)$$

The strands are electrically connected to each other at the end of the cable. Since the contact resistance at element $i = n_{max}$ is null, Eq. (4.3) is rewritten as

$$R_{(1,n_{max})}I_{(1,n_{max})} - R_{(2,n_{max})}I_{(2,n_{max})} - R_cI_{c(n_{max}-1)} + \sum_{j,k=1,0}^{2,n}\left\{(M_{(1,n_{max})(j,k)} - M_{(2,n_{max})(j,k)})\frac{dI_{(j,k)}}{dt}\right\} = 0. \quad (4.7)$$

From these simultaneous differential equations, the current at each element is obtained at every time step by the Runge-Kutta method which provides numerical solutions for differential equations.

The Joule heat generation at the contact conductance is calculated from $I_c$. The equation is given by

$$\begin{aligned} g_{c(i)} &= \frac{1}{A\Delta l}\left(\frac{R_cI_{c(i)}^2}{4} + \frac{R_cI_{c(i+1)}^2}{4}\right) \\ &= \frac{1}{A\Delta l}\left(\frac{I_{c(i)}^2}{4\sigma_c\Delta l} + \frac{I_{c(i+1)}^2}{4\sigma_c\Delta l}\right), \end{aligned} \quad (4.8)$$

where $\Delta l$ is the element length and $\sigma_c$ is the electrical contact conductance between the strands per unit length.

### 4.2.3 Parameters

#### (a) Critical current and temperature

For the critical temperature of NbTi, $T_c$, we consider the dependence of an external magnetic field. $T_c$ at the external magnetic field $B$ and the current density of 0 A/m$^2$ is given by

$$T_c(B) = T_{c0}\left(1 - \frac{B}{B_{c0}}\right)^{0.59}, \quad (4.9)$$

where $T_{c0}$ is the critical temperature for the external magnetic field of 0 T and the current density of 0 A/m$^2$, and $B_{c0}$ is the critical magnetic field at 0 K and the current density of 0 A/m$^2$.

The critical current density of NbTi, $J_{c,NbTi}$, depends on the temperature and external magnetic field. For the calculation of $J_{c,NbTi}$, we used approximate equations derived by G. Morgan [39] and M. A. Green [40]. These equations need the standard value of $J_c$. In the present calculation, the value of $J_{c,NbTi}$ was selected so that the critical current of the strand at 4.3 T and 4.22 K was 400 A. The critical current of the strand, $I_{c,strand}$ at 4.22 K as a function of external magnetic field is shown in Fig. 4.3(a), and Fig. 4.3(b) shows $I_{c,strand}$ as a function of temperature at 3.7 T, 4.0 T and 4.3 T.

Transition between normal and superconducting states will be described in Section (c).

### (b) Specific heat

The specific heat [J/m$^3$K] of a strand is given by

$$C_p = \frac{\alpha}{1+\alpha} C_{p,Cu}(T) + \frac{1}{1+\alpha} C_{p,NbTi}(T, B), \tag{4.10}$$

where $\alpha$ is the Cu/Sc ratio, $C_{p,Cu}$ is the specific heat of copper, and $C_{p,NbTi}$ is the specific heat of NbTi.

The specific heat of copper varies depending on the temperature. For $T < 15$ K, the equation for $C_{p,Cu}$ is given by

$$C_{p,Cu}(T) = 2.4T^3 + 105T^{1.2}. \tag{4.11}$$

The specific heat of NbTi depends on the temperature and external magnetic field, and is given by

$$C_{p,NbTi}(T, B) = 58.09T^3 + 99.68TB \qquad (T < T_c(B)) \tag{4.12}$$

$$C_{p,NbTi}(T, B) = 37.08T^3 + (49.84B + 505.89)T \qquad (T = T_c(B)) \tag{4.13}$$

$$C_{p,NbTi}(T, B) = 16.07T^3 + 1011.78T \qquad (T_c(B) < T < 10K) \tag{4.14}$$

Figure 4.4 shows an example of the specific heat of the strand. For the temperature range except for those described above, the interpolated values based on *NIST* (the National Institute of Standards and Technology) data were used.

### (c) Resistivity

Assuming a strand as a parallel circuit made of a NbTi wire and a copper wire, the resistivity of the strand is given by

$$\frac{1}{\rho} = \frac{\alpha}{(1+\alpha)\rho_{Cu}} + \frac{1}{(1+\alpha)\rho_{NbTi}} \tag{4.15}$$

where $\rho_{Cu}$ and $\rho_{NbTi}$ are the resistivities of copper and NbTi, respectively. They depend on temperature and external magnetic field. This equation is rewritten as

$$\rho = \frac{(1+\alpha)\cdot\rho_{Cu}(T,B)\cdot\rho_{NbTi}(T,B)}{\rho_{Cu}(T,B)+\alpha\rho_{NbTi}(T,B)}. \tag{4.16}$$

The equation for $\rho_{Cu}$ is given by

$$\rho_{Cu}(T,0)=A_1+A_2+A_3, \text{ and} \tag{4.17}$$

$$\rho_{Cu}(T,B)=(1+10^{A_4})\rho_{Cu}(T,0), \tag{4.18}$$

$$\text{where} A_1=\frac{15.53\times10^{-9}}{RRR},$$

$$A_2=\frac{1.171\times10^{-17}T^{4.49}}{1+4.50\times10^{-7}T^{3.35}\exp\left(-(50/T)^{6.428}\right)},$$

$$A_3=0.4531\frac{A_1A_2}{A_1+A_2},$$

$$A_4=-2.662+0.3168A_5+0.6229A_5^2-0.1839A_5^3+0.01827A_5^4,$$

$$A_5=\frac{\ln(15.53\times10^{-19}B/\rho_{Cu}(T,0))}{\ln 10}.$$

$RRR$ is the residual resistivity ratio of copper.

The equation for $\rho_{NbTi}$ is given by

$$\rho_{NbTi}(T,B)=\rho_0\left(\frac{J_{NbTi}}{J_{c,NbTi}(T,B)}\right)^n\equiv\rho_0\left(\frac{I_{strand}}{I_{c,strand}}\right)^n \tag{4.19}$$

where $\rho_0$ is the resistivity to define the critical current density, $n$ is the $n$-value of the superconductor, and $J_{NbTi}$ is the current density in the superconductor, NbTi. In the

present study, $\rho_0$ is $1 \times 10^{-14}$ [$\Omega$m], and the $n$-value is 70. In the calculation, the maximum $\rho_{NbTi}$ is defined to be $5.6 \times 10^{-7}$ [$\Omega$m], and all the resistivity above this value is regarded as this constant value. The resistivity of $5.6 \times 10^{-7}$ [$\Omega$m] is the resistivity of NbTi in the normal state.

As an example of the strand resistivity, Fig. 4.5 shows the strand resistivity at the strand current of 350 A.

In the following calculation, the distinction between the superconducting and normal states of the strand was done by resistivity. The normal state was defined as a state whose resistivity was higher than $1 \times 10^{-14}$ $\Omega$m.

### (d) Thermal conductivity

Since the thermal conductivity [W/mK] of NbTi is less than 1/100 of the thermal conductivity of copper, it is neglected. The thermal conductivity of the strand is given by

$$\kappa = \frac{\alpha}{1+\alpha}\kappa_{cu}(T, B), \tag{4.20}$$

where $\kappa_{Cu}$ is the thermal conductivity of copper, which depends on temperature and magnetic field. $\kappa_{Cu}$ is calculated from the Wiedemann-Franz-Lorentz law,

$$\kappa_{Cu} = \frac{L_0 T}{\rho_{Cu}(T, B)}, \tag{4.21}$$

where $L_0$ is the Lorentz number, $L_0 = 2.44 \times 10^{-8}$ [W$\Omega$/K$^2$], and $\rho_{Cu}$ is the resistivity of copper. Fig. 4.6 shows an example of the thermal conductivity of the strand. In the temperature range from the temperature of the peak thermal conductivity to 50 K, the Wiedemann-Franz-Lorentz law is not valid. However, the simulation of quench propagation is not influenced by this discrepancy, since the temperature range critical to the quench propagation is mainly from liquid helium temperature to about 20 K.

### (e) Inductance

In the calculation, one element is taken as a thin wire except for the calculation of self inductance. For the inductance calculation, we refer to reference [41].

As shown in Fig. 4.7, the self inductance of wire element is calculated by the following equation

$$L = \frac{\mu_0 l}{2\pi}\left\{\ln\left(\frac{2l}{r}\right) - \frac{3}{4}\right\}, \tag{4.22}$$

where $l$ and $r$ are the length and radius of a wire element, respectively.

The mutual inductance between two parallel wires, as shown in Fig. 4.7(b), is calculated by

$$M_{parallel} = \frac{\mu_0 l}{2\pi}\left\{\ln\left(\frac{l+\sqrt{l^2+h^2}}{h}\right) - \frac{\sqrt{l^2+h^2}}{l} + \frac{h}{l}\right\}. \tag{4.23}$$

The mutual inductance between coaxial wires, as shown in Fig. 4.7(c), is calculated by

$$\begin{aligned} M_{coaxial} = \frac{\mu_0}{4\pi}\{&(l_1+l_2+d)\ln(l_1+l_2+d) \\ &-(l_1+d)\ln(l_1+d) - (l_2+d)\ln(l_2+d) + d\ln d\}. \end{aligned} \tag{4.24}$$

The mutual inductance, as shown in Fig. 4.7(d), is calculated by

$$\begin{aligned} M = \frac{1}{2}\{&M_{parallel}(l_1+l_2+d,h) - M_{parallel}(l_1+d,h) \\ &-M_{parallel}(l_2+d,h) + M_{parallel}(d,h)\}. \end{aligned} \tag{4.25}$$

### (f) Magnetic field

The actual Rutherford cable is twisted, and the field distribution exists across the cable cross section as shown in Fig. 4.8(a). Therefore a strand is exposed to a periodic magnetic field. For the two-parallel strand model, the magnetic field distribution is applied to each element as shown in Fig. 4.8(b). The maximum and minimum fields are alternately applied to the element. $B_{max}$ and $B_{min}$ are defined by Eqs. (2.3) and (2.4), respectively.

## 4.3 Results

### 4.3.1 Quench Propagation Velocity

As the initial condition for calculations at time $t = 0$, the following temperature distributions were supplied to the cable; a portion of 15.5 mm of the center of strand 1 was at 9.2 K, and the other region was at 4.2 K. The element length, $\Delta l$, was 3.875 mm. The initial current distribution was assumed to be uniform.

An example of quench propagation is shown in Fig. 4.9, where the strand current was 387.5 A and the contact electrical conductance, $\sigma_c$, was $2.5\times10^7$ S/m. The horizontal axis is time $t$, and the vertical axis is the quench front position $x$. The cable center is at $x = 0$. From Fig. 4.9(a), the normal zone propagates with constant velocity. As shown in Fig. 4.9(b) which is a magnified figure of Fig. 4.9(a), at the time interval from 2.6 to 3.0 msec, the quench front of strand 1 propagated faster than the quench front of strand 2. On the other hand, at the time interval from 3.0 to 3.4 msec, the quench front of strand 2 propagated faster than the quench front of strand 1. The alternating propagation of the quench front like this was caused by the magnetic field distribution. The strand was in the maximum and minimum magnetic fields in turns over a half of the cable twist pitch. For instance, in the region from $x$ =124 mm to 139.5 mm, the field of strand 1 was $B_{max}$, and for the next half pitch, in the region of $x$ =139.5 to 155 mm, the field was $B_{min}$. For strand 2, the reverse fields were applied. Since the quench propagation at the high field region was faster than that of the low field region, the quench fronts of strands 1 and 2 propagated alternately.

Figure 4.10 shows the quench propagation velocities for three electrical contact conductance, $\sigma_c = 2.5 \times 10^5$, $2.5 \times 10^7$ and $2.5 \times 10^{10}$ S/m . These conditions correspond to low contact cable, original cable and high contact cable, respectively, used in the Rutherford cable tests described in Chapter 2. The horizontal axis is the strand current and the vertical axis is the quench propagation velocity, which corresponds to the slope of the quench propagation curve, such as Fig. 4.9(a), obtained by the least squares method. Comparing this figure with Fig. 2.15, we can see that the curves were similar to each other. From Fig. 4.10, in the lower current range, the difference of the velocities

of three conditions were small. In the higher current range, the velocities of the cable with high contact conductance were higher than those of the cable with low contact conductance.

The quench propagation velocity as a function of $\sigma_c$ is shown in Fig. 4.11, where the strand current was 387.5 A. The calculated quench propagation velocity of a single strand with the same magnetic field distribution was 33.9 m/s, and the velocity taking into account the current redistribution between strands is higher than the velocity of a single strand without the current redistribution. This fact suggests that the current redistribution increased the quench propagation velocity in the cable made of non-insulated strands. Fig. 4.11 also indicates that the influence of the current redistribution on the quench propagation velocity will become larger as the electrical contact conductance increases, and in the region above $\sigma_C = 1 \times 10^9$ S/m, the velocity was essentially independent of the electrical contact conductance.

### 4.3.2 Current Redistribution

The current redistribution is compared with the cable test results. Fig. 4.12 shows the current change of strand 1 at 387.5 A and $x = 240.3$ mm, in which strands 1 and 2 were placed in $B_{min}$ and $B_{max}$, respectively. $\sigma_c$ was $2.5 \times 10^7$ S/m, which corresponds to original cable in the cable tests. In this figure, the position of the quench front is also plotted. As shown in this figure, when the quench front passed through at about $t = 6$ msec, the current of about 35.4 A transferred from strand 2 in the high field to strand 1 in the low field, and then the current of about 25.7 A returned to strand 2 from strand 1 immediately. Such a current redistribution was quite similar to the result of original cable in the Rutherford cable tests as shown in Fig. 2.24. In Fig. 2.24, the reason why the signal width at $t_{fcr}$ was broad in comparison with the calculated results seems to be the influence of a low pass filter of the differential amplifier.

The current change of strand 1 for $\sigma_c = 2.5 \times 10^5$ S/m and $x = 240.3$ mm is shown in Fig. 4.13. Although the time when the quench front reached to this position was about 6.5 msec, the current changed periodically before that time. The characteristic of

current redistribution is also quite similar to that of the results of low contact cable in the cable tests. The dotted line in Fig. 4.13 represents the magnetic field at the quench front position of strand 1. The periodicity of the magnetic field at the quench front almost agreed with that of the current oscillations. This fact indicates that the periodic current changes in the cable with low contact conductance is caused by the periodic distribution of the magnetic field due to the twist of the cable.

This mechanism can be explained as follows. The region, where the current redistribution occurs, spreads as the electrical contact conductance decreases. For simplicity, we discuss a sinusoidal wave circuit as shown in Fig. 4.14. Line segments AB and A'B' are in contact with each other continuously, and complex voltage source and impedance $Z_L$ are connected at the ends AA' and BB', respectively. $I_{sw}(x)$ is given by [42]

$$I_{sw}(x)=\frac{1}{Z_c}(A_{sw}e^{-(\alpha_{sw}+j\beta_{sw})x}) \qquad (x>0) \tag{4.26}$$

$$Z_c=\sqrt{\frac{Z}{Y}} \tag{4.27}$$

$$Z=R_{sw}+j\omega L_{sw} \tag{4.28}$$

$$Y=G_{sw}+j\omega C_{sw} \tag{4.29}$$

where $A_{sw}$ is an arbitrary constant, $R_{sw}$ is the series resistance per unit length [$\Omega$/m], $L_{sw}$ is the distributed series inductance per unit length [H/m], $G_{sw}$ is the parallel conductance per unit length [S/m], and $C_{sw}$ is the distributed parallel capacitance per unit length [F/m]. And $\alpha$ and $\beta$ are called *attenuation constant* and *phase constant*, respectively. They are given by

$$\alpha_{sw}=\frac{1}{\sqrt{2}}\sqrt{\sqrt{(R_{sw}^2+\omega^2L_{sw}^2)(G_{sw}^2+\omega^2C_{sw}^2)}+(R_{sw}G_{sw}-\omega^2L_{sw}C_{sw})} \tag{4.30}$$

$$\beta_{sw}=\frac{1}{\sqrt{2}}\sqrt{\sqrt{(R_{sw}^2+\omega^2L_{sw}^2)(G_{sw}^2+\omega^2C_{sw}^2)}-(R_{sw}G_{sw}-\omega^2L_{sw}C_{sw})} \tag{4.31}$$

From Eq. (4.26), the amplitude of $I_{sw}(x)$ decreases in proportion to $e^{-\alpha_{sw}x}$. In order to decreases the amplitude in short length, the larger $\alpha_{sw}$ is preferable.

In the numerical simulation of the quench propagation, $L_{sw}$ and $C_{sw}$ were assumed to be constant, and $R_{sw}$ was determined by the strand resistivity and the element length. As the contact conductance, $G_{sw}$, increases, the attenuation constant, $\alpha_{sw}$, increases, namely, the current redistribution occurs in a smaller region.

Fig. 4.15 shows the calculated length from the quench front to the element, where the influence of the current change at the quench front appears. The strand current was at 387.5 A. The horizontal axis is the electrical contact conductance and the vertical axis is the length between the quench front and the element of the current change more than 0.1 A. We can see from this figure that, the region of the current redistribution decreases with the electrical contact conductance, and in the conductance region above $1 \times 10^8$ S/m, the region remains constant at 7.75 mm.

From the above equations, the region of the current redistribution decreases with increasing contact conductance. However, as shown in Fig. 4.15, the region of the current redistribution remains to be a constant length for $\sigma_c > 1 \times 10^8$ S/m. The reason for this is the inductance coupling between elements and the finite element length. When the current changes near the element of interest, the inductive voltage is induced and the current changes at the element.

As seen from Fig. 4.15, in the conductance range below $1 \times 10^8$ S/m, the region of the current redistribution is large. Namely, the influence of the current change appears even at a long distant element. For example, when the current transfers from strand 1 to strand 2 at the quench front, the current transfer from strand 1 to strand 2 occurs quite faraway from the quench front.

The current change at the quench front occurs basically from the high field region to the low field region. When the magnetic field distribution changes periodically along the route of the quench front, the current at the element which is quite distant from the quench front also changes periodically depending on the current change at the quench front. Fig. 4.16 shows the current changes at $\sigma_c = 2.5 \times 10^5$ S/m and $x = 240.3$ mm for two twist pitches. The solid and dashed lines represent the current changes for twist pitches of 31 mm and 62 mm, respectively. We can see from this figure that the period of the current change is approximately proportional to the length of the twist pitch. The periodic times of the current changes for twist pitches of 31 mm and 62 mm were 0.82 msec and 1.63 msec, respectively, and the quench propagation velocities were 34.46 m/sec and 34.44 m/s, respectively.

Figure 4.17 shows the current change of strand 1 at $x = 240.3$ mm and for $\sigma_c =$

$2.5 \times 10^{10}$ S/m. This electrical conductance corresponds to high contact cable in the Rutherford cable tests. Let us compare the calculated results in this figure with the test results shown in Fig. 2.24. The current change occurred only once in the cable tests, while in the calculation results the current change occurred twice. This discrepancy was due to the difference between the simulation model and the actual Rutherford cable. In the two-parallel strand model for the calculation, the heat conduction between strands was neglected. However, the heat conduction actually influenced the current redistribution and quench propagation. Especially for high contact cable in the cable tests, since the cable was impregnated with solder, the thermal conductivity between strands was very high and its influence could not be neglected.

In order to estimate the effects due to the thermal conductivity between strands, a calculation taking account of the heat conduction between strands was performed. In this case, by adding the heat conduction term in Eq. (4.1), the thermal equilibrium equation is given by

$$\frac{\partial}{\partial x}\left(\kappa\frac{\partial T}{\partial x}\right) + g + g_c + \frac{p_{cn}}{A} = C_p\frac{\partial T}{\partial t}, \tag{4.32}$$

where $p_{cn}$ is the heat conduction between strands. In the calculation, it was difficult to estimate the heat conduction between strands, since the measurement of thermal conductivity among strands was very difficult and since there were little experimental data available [43]. Therefore, in the present study, we used an approximate equation in which the heat conduction between strands was assumed to be proportional to the temperature difference between the strands. The heat conduction from strand 1 to strand 2 is given by

$$p_{cn} = h_{const} \times (T_2 - T_1), \tag{4.33}$$

where $h_{const}$ is the constant thermal conductivity between strands 1 and 2, and $T_1$ and $T_2$ are the temperatures of strands 1 and 2, respectively. The calculated results using the above equation for various values of $h_{const}$, 0, 100 and 500 W/mK, are shown in Fig. 4.18, where $\sigma_c = 2.5 \times 10^{10}$ S/m and the strand current was 387.5 A. From this figure, as the thermal conductivity between strands increases, the peak of the current

change becomes low. The reason for this will be discussed in the next chapter.

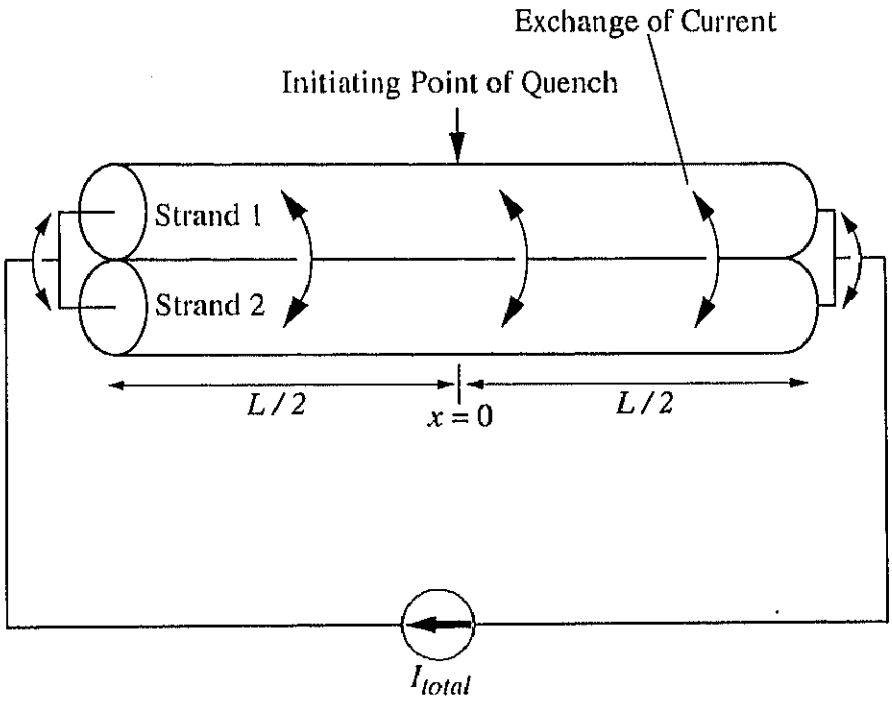


Fig. 4.1: Two-parallel strand model.

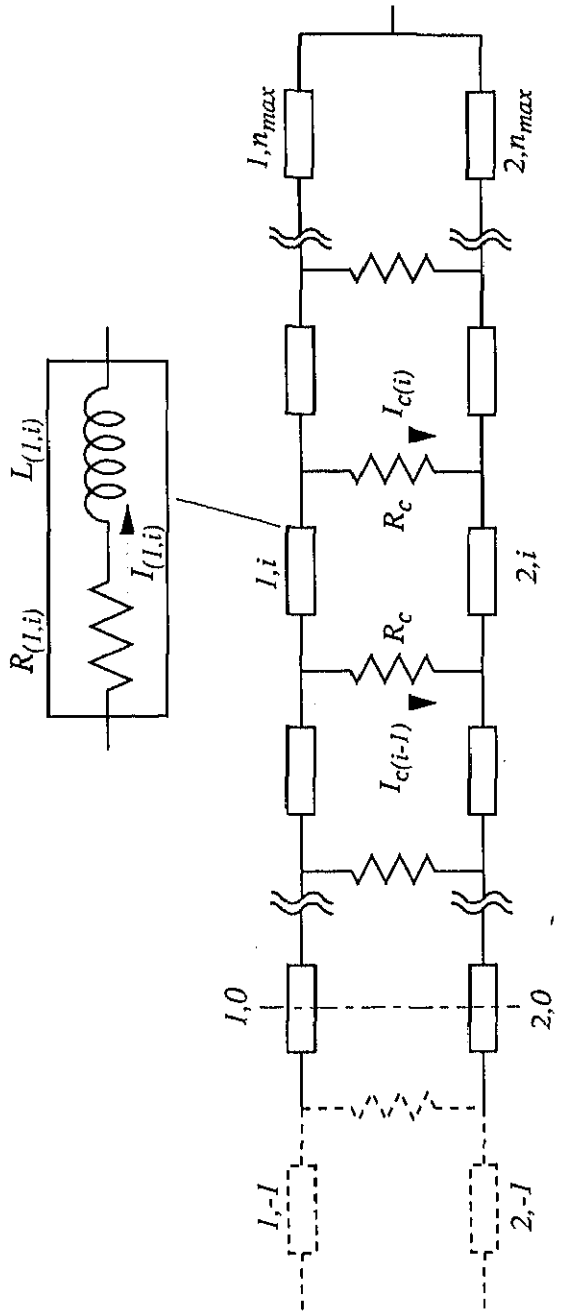


Fig. 4.2: Electrical circuit model of two-parallel strands.

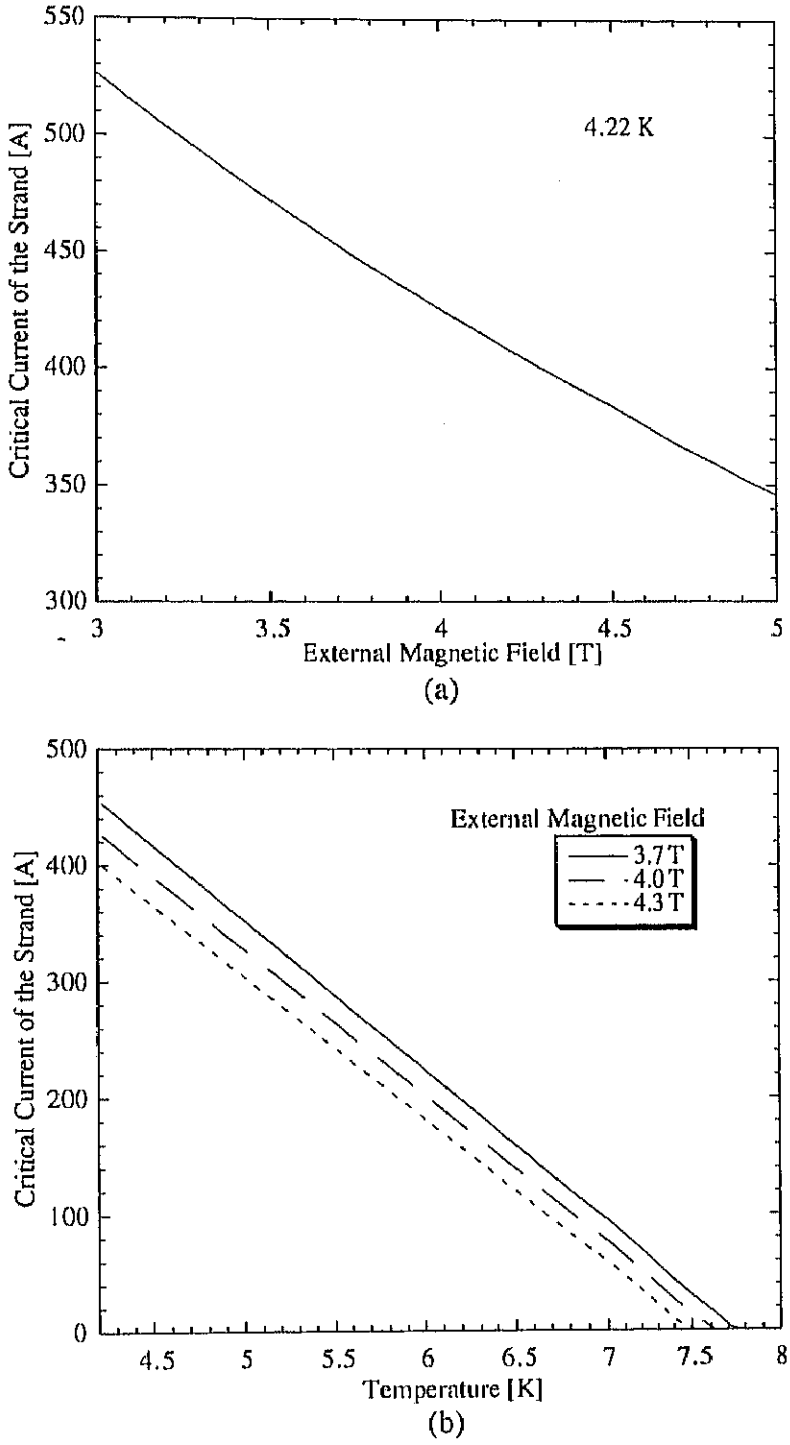


Fig. 4.3: Example of critical current of the strand.

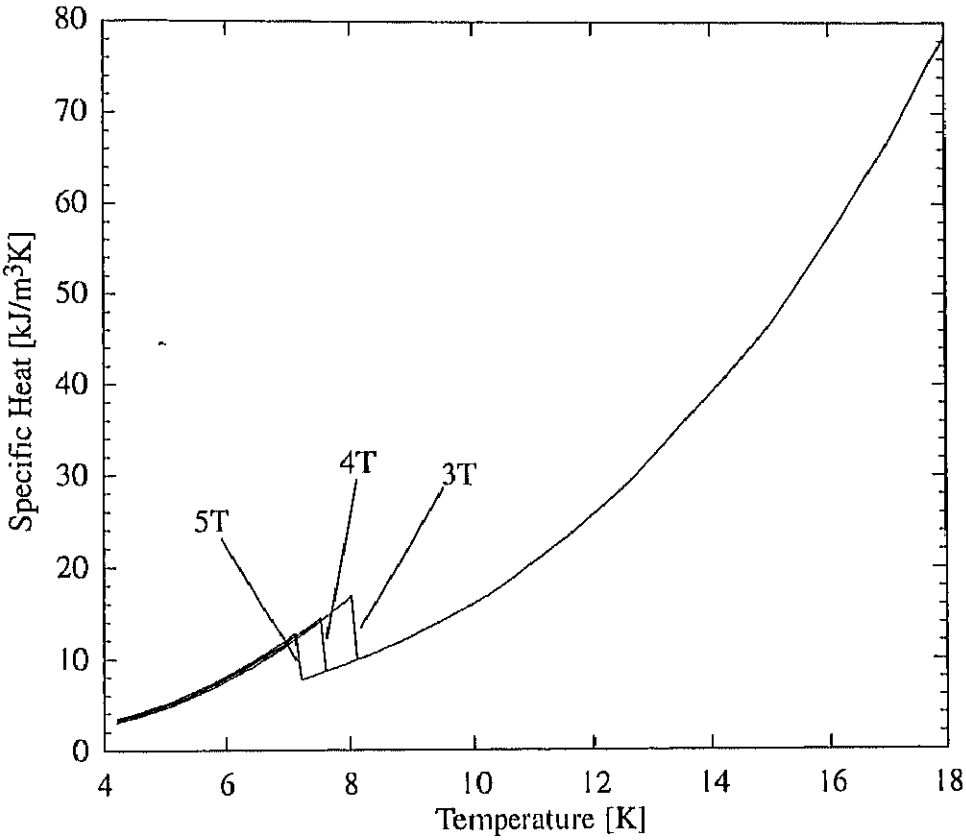


Fig. 4.4: Example of the specific heat of the strand.

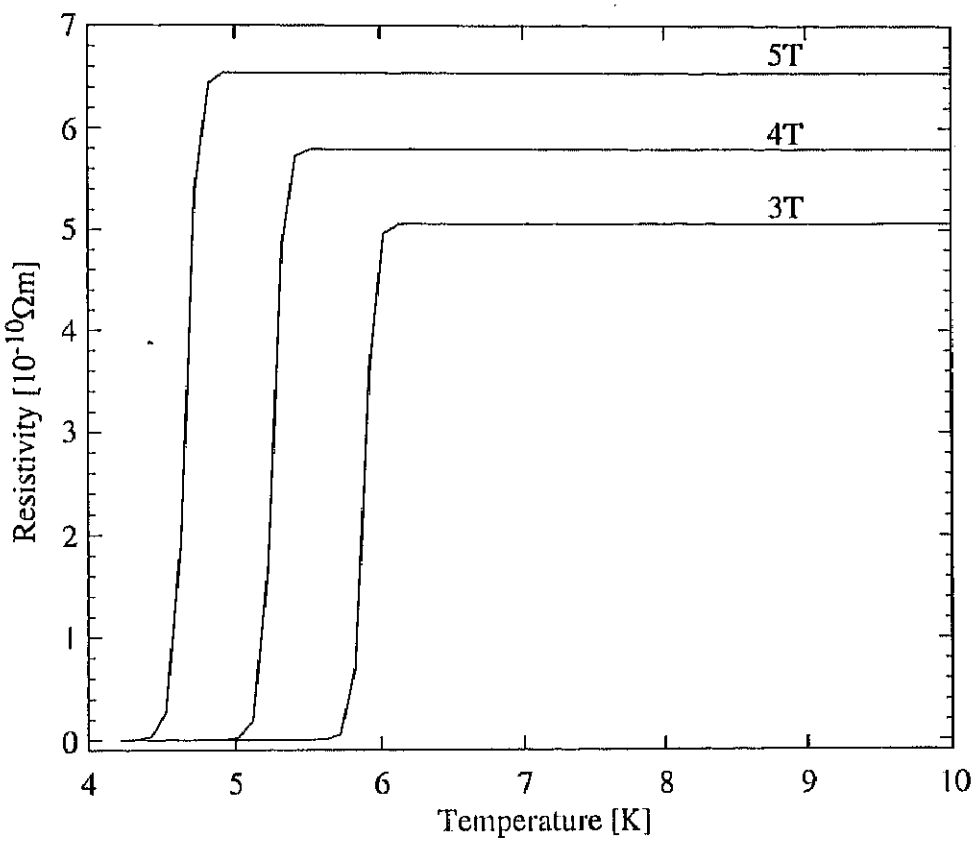


Fig. 4.5: Example of the resistivity of the strand. The strand current is 350 A.

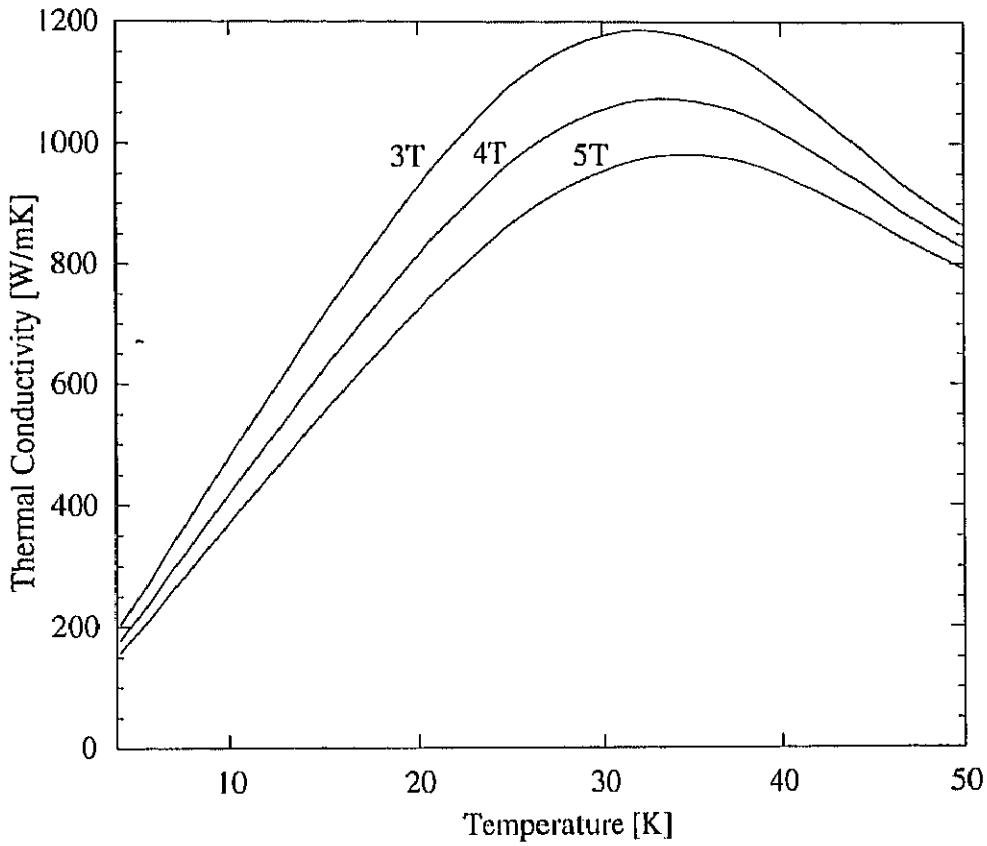


Fig. 4.6: Example of the thermal conductivity of the strand.

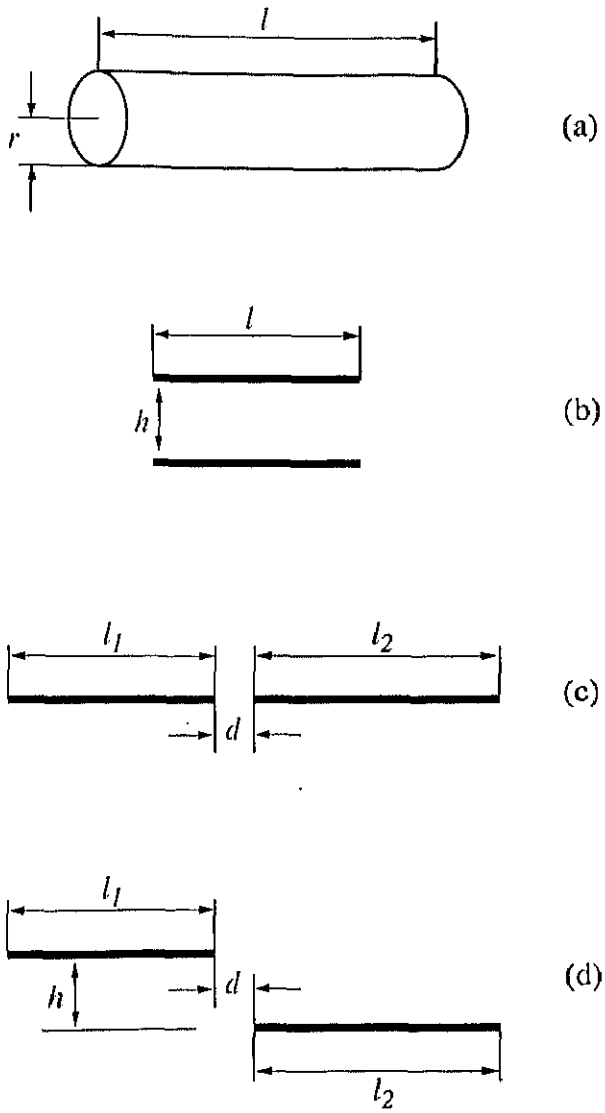


Fig. 4.7: Relative positions of wire elements for the inductance calculation.

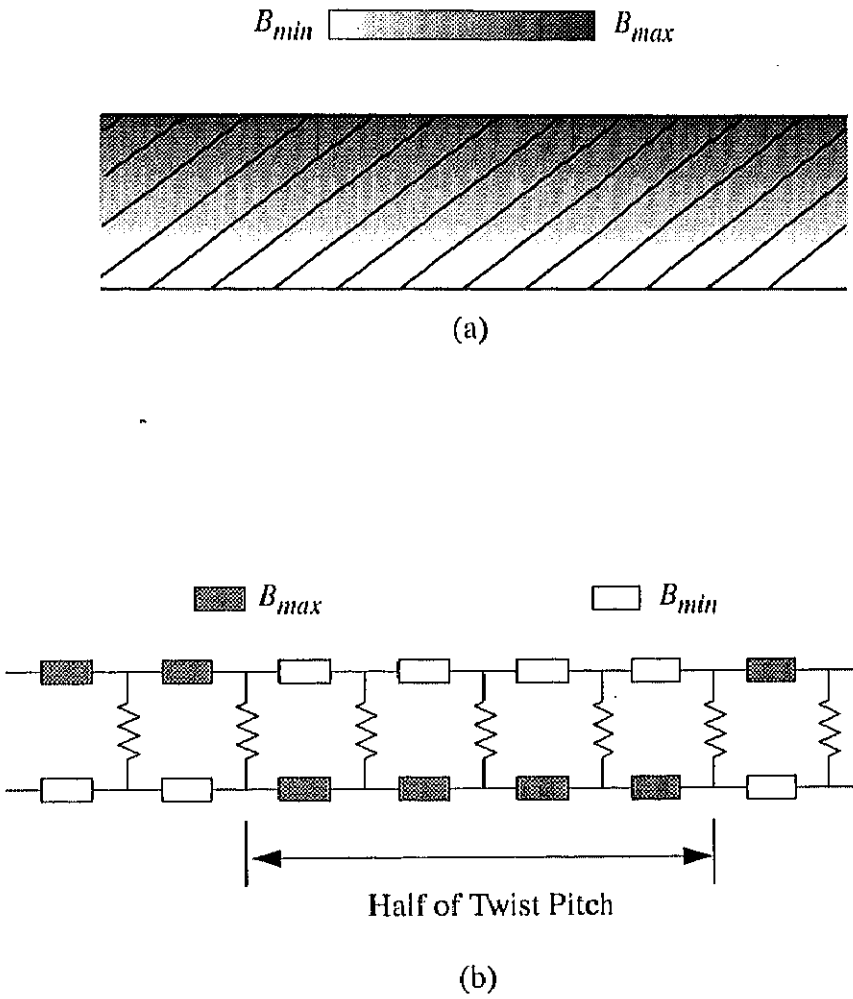


Fig. 4.8: Field distribution of the Rutherford cable and the two-parallel strand model.

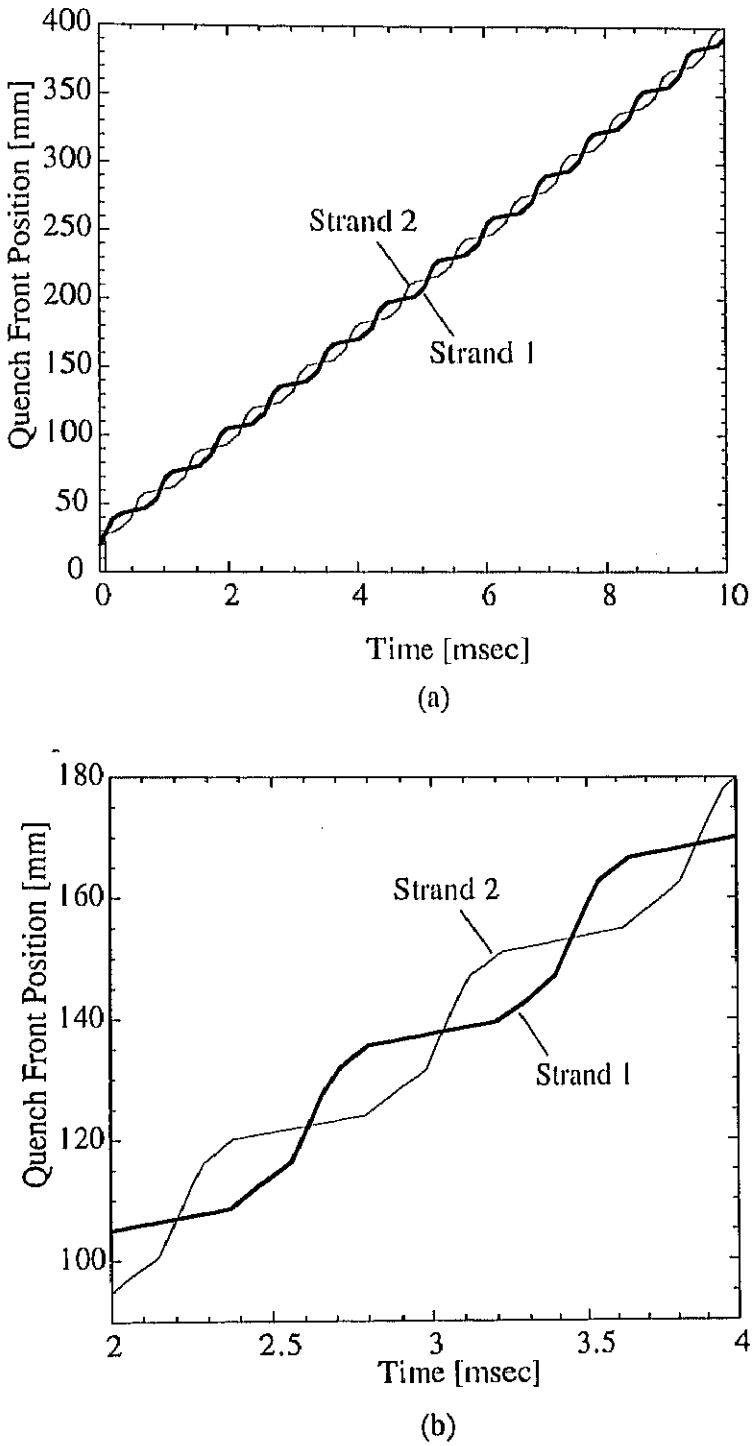


Fig. 4.9: Example of quench propagation in strands 1 and 2.

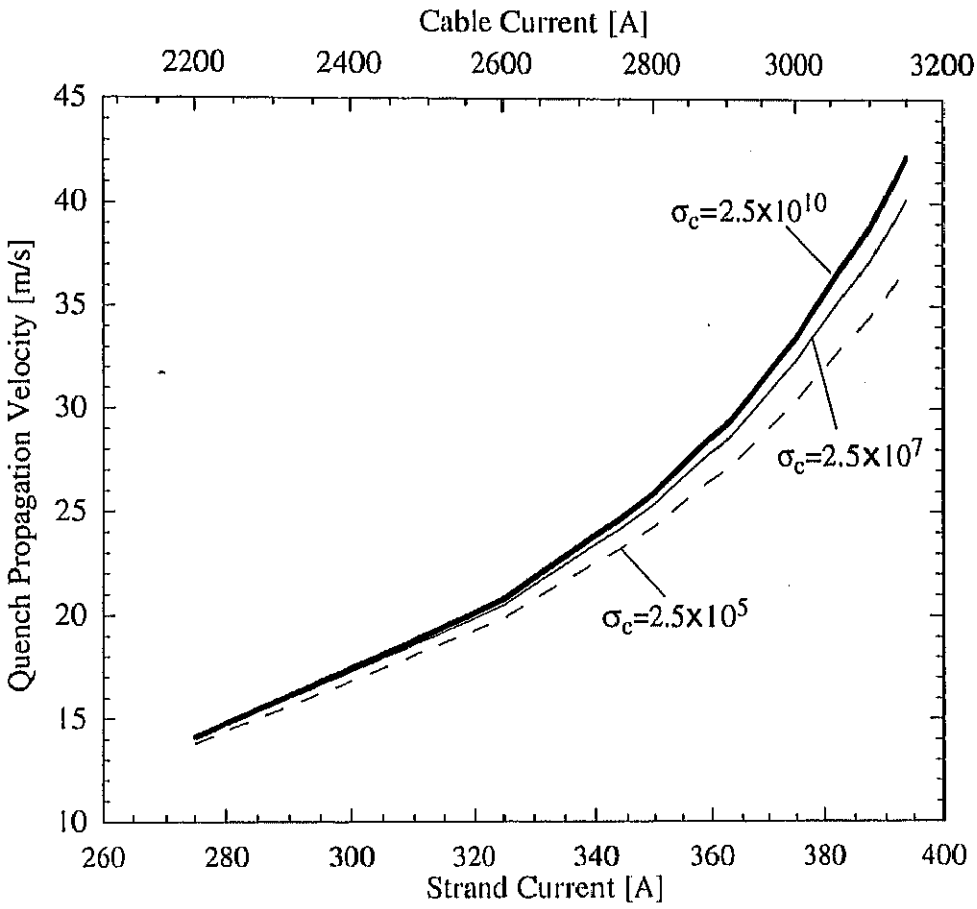


Fig. 4.10: Calculated quench propagation velocities as a function of strand current.

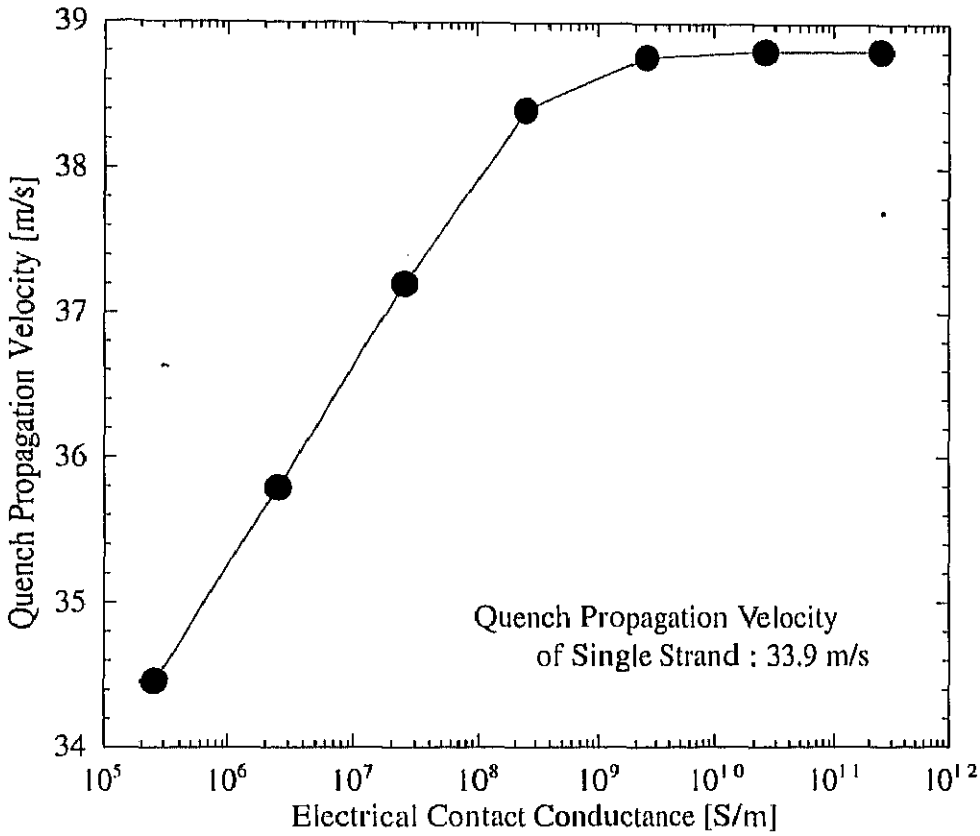


Fig. 4.11: Quench propagation velocity as a function of electrical contact conductance at the strand current of 387.5 A.

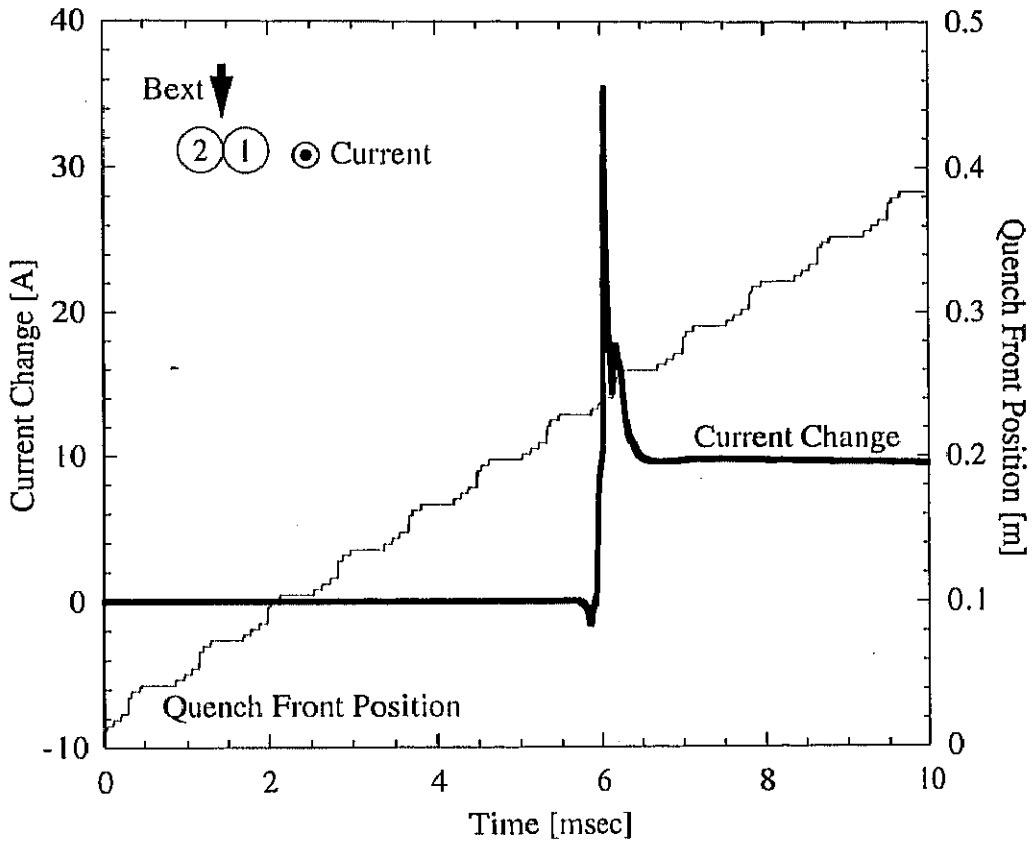


Fig. 4.12: Calculated current change and quench front position of strand 1 at 387.5 A, $x = 240.3$ mm and $\sigma_c = 2.5 \times 10^7$ S/m.

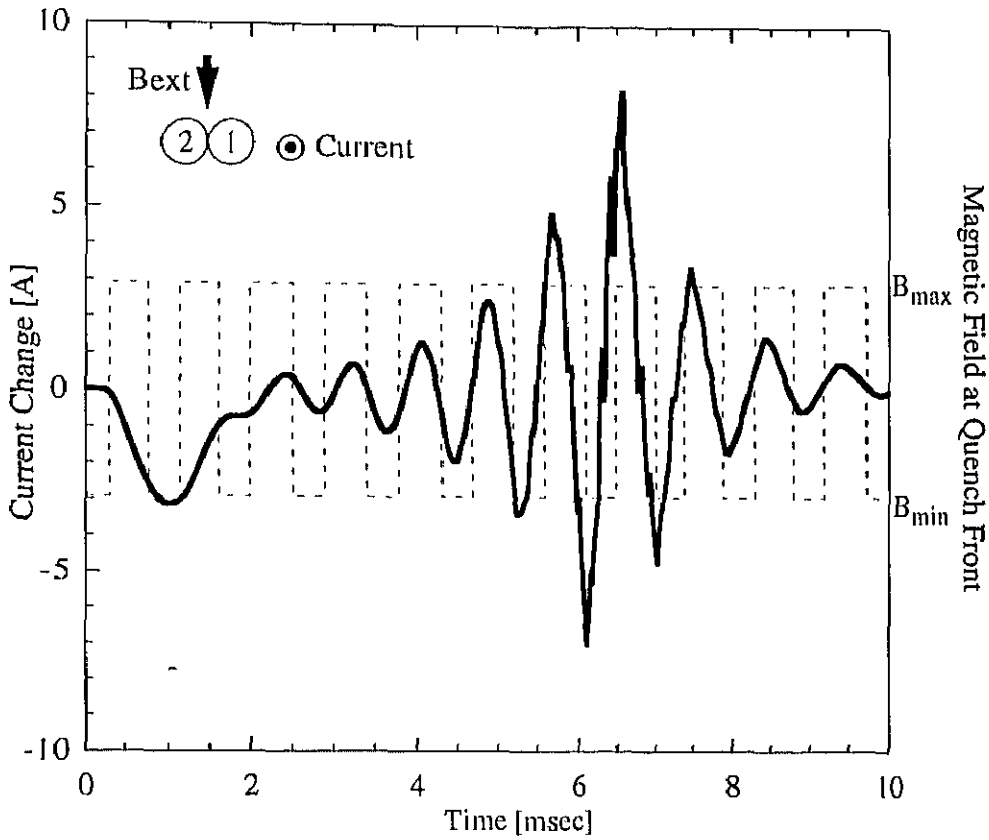


Fig. 4.13: Calculated current change of strand 1 at the strand current of 387.5 A, $x = 240.3$ mm and $\sigma_c = 2.5 \times 10^5$ S/m. The dotted line represents the magnetic field at the quench front position of strand 1.

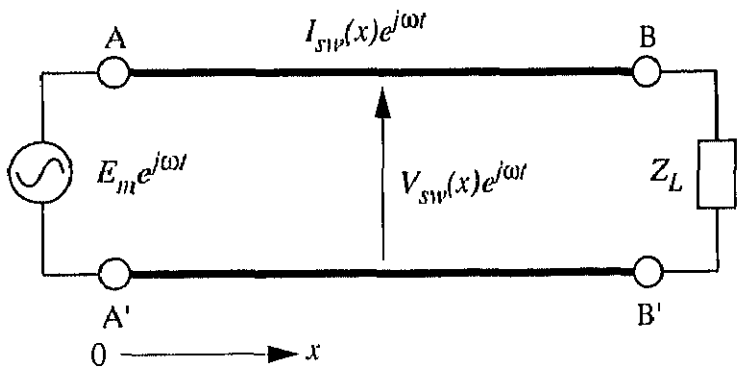


Fig. 4.14: Sinusoidal wave circuit.

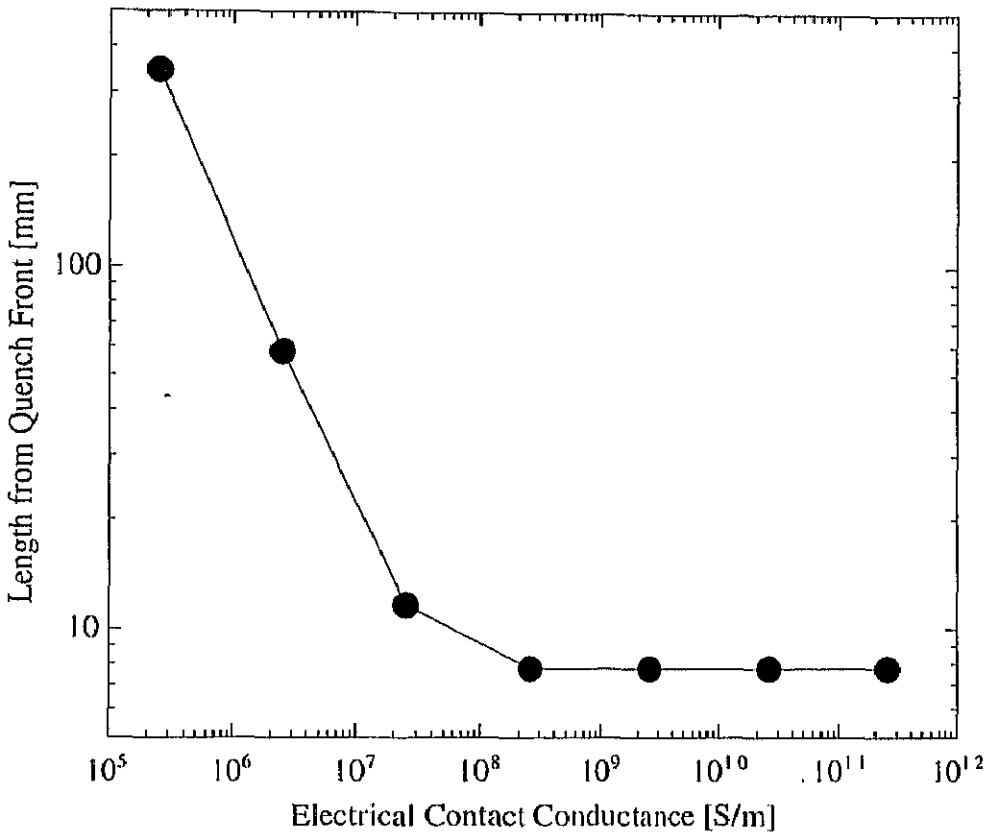


Fig. 4.15: Region of the current redistribution calculated at the strand current of 387.5 A. The vertical axis is the calculated length between the quench front and the element that the current changes more than 0.1 A.

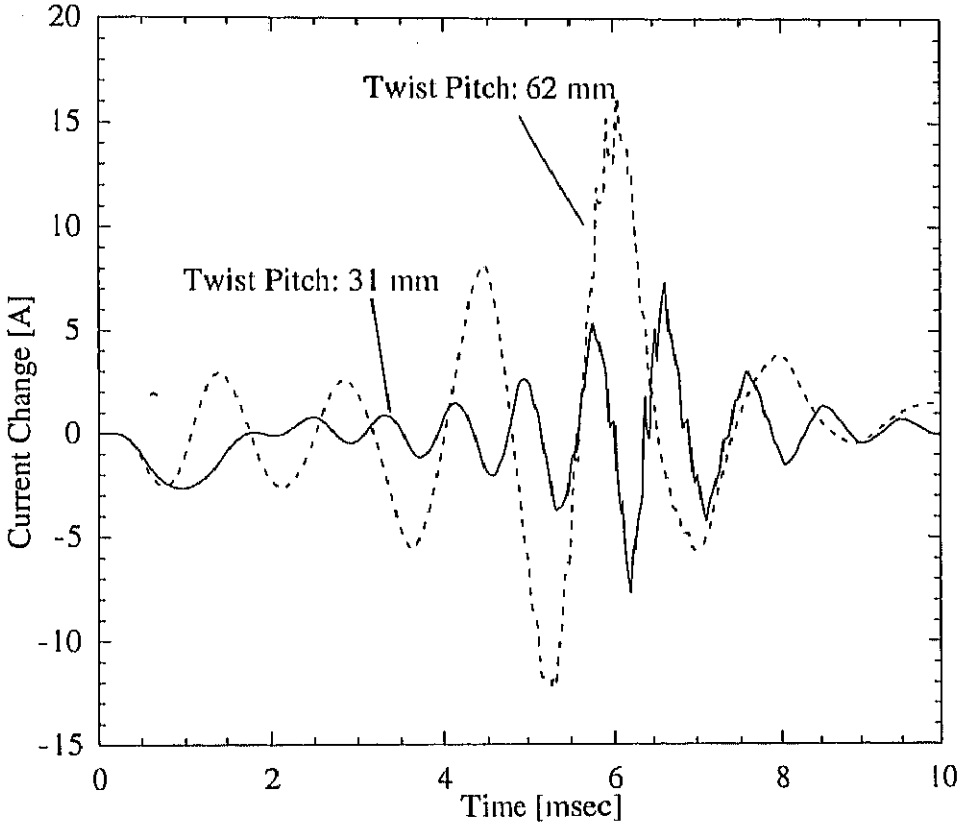


Fig. 4.16: Calculated current changes in two twist pitches, where $\sigma_c = 2.5 \times 10^5$ S/m and $x = 240.3$ mm. The solid and dashed lines represent the current changes in the twist pitch of 31 mm and 62 mm, respectively.

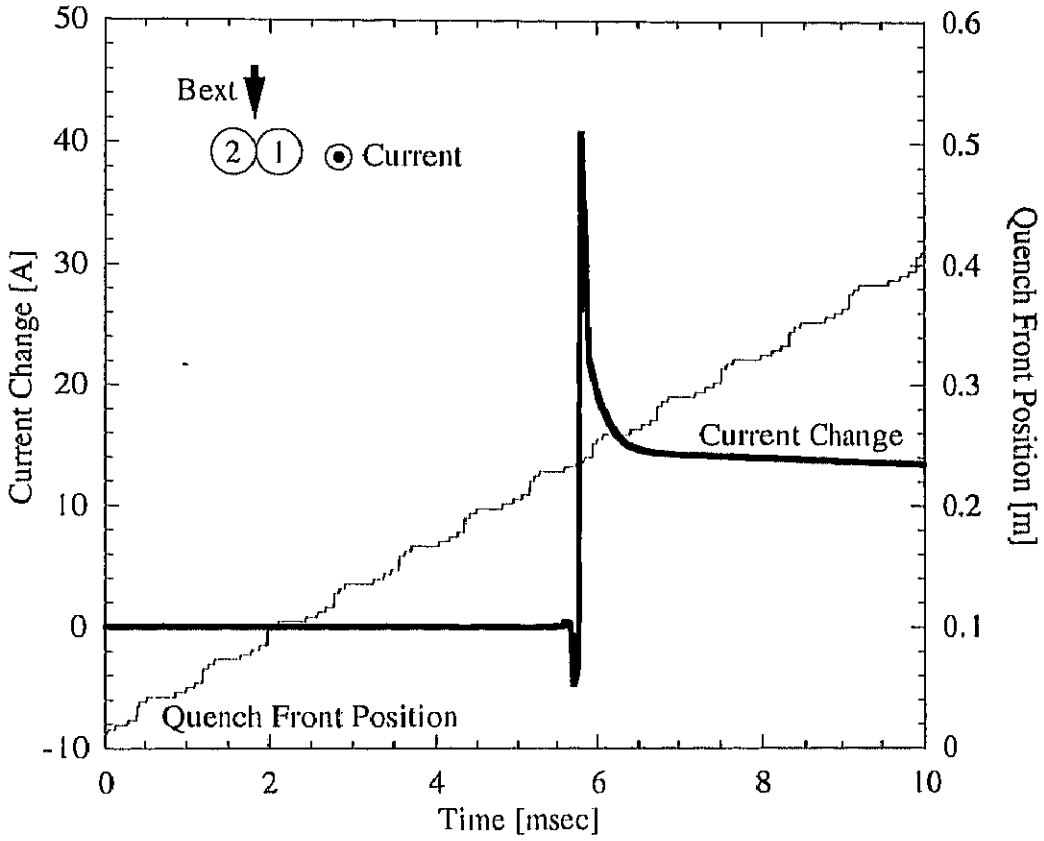


Fig. 4.17: Calculated current change and quench front position of strand 1 at the strand current of 387.5 A, $x = 240.3$ mm and $\sigma_c = 2.5 \times 10^{10}$ S/m.

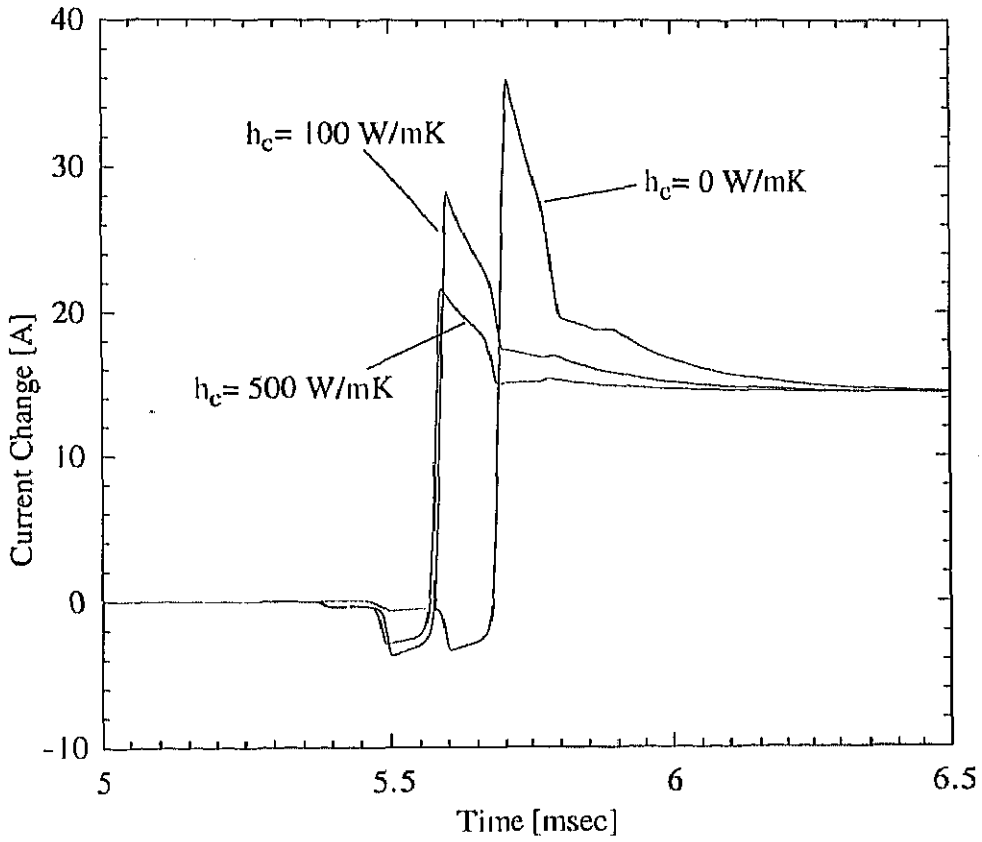


Fig. 4.18: Calculated current changes of strand 1 for three thermal conductivities between strands for the strand current of 387.5 A, $x = 240.3$ mm and $\sigma_c = 2.5 \times 10^{10}$ S/m.